# Quasi-monochromatic ULF foreshock waves as observed by the four-spacecraft Cluster mission: 1. Statistical Properties

J. P. Eastwood, A. Balogh, E. Lucek, C. Mazelle, J. Dandouras

# Quasi-monochromatic ULF foreshock waves as observed by the four-spacecraft Cluster mission: 1. Statistical properties

J. P. Eastwood

Laboratory for Solar and Space Physics, Geospace Physics Branch, NASA Goddard Space Flight Center, Greenbelt, Maryland, USA

A. Balogh and E. A. Lucek

Space and Atmospheric Physics, Blackett Laboratory, Imperial College London, London, UK

C. Mazelle and I. Dandouras

Centre d'Etude Spatiale des Rayonnements, Centre National de la Recherche Scientifique, Toulouse, France

Received 7 June 2004; revised 7 July 2005; accepted 18 July 2005; published 26 November 2005.

[1] Cluster data are used to study the statistics of a particular type of foreshock wave: quasi-monochromatic ultra-low-frequency (ULF) waves with characteristic periods of 30 s in the spacecraft frame. On the basis of a large set of foreshock observations made in 2001 with spacecraft separations ~600 km, the intrinsic properties of the waves are found using a cross-correlation timing analysis. This method, which allows the solar wind rest frame properties of the waves to be calculated with fewer assumptions when compared to previous dual spacecraft analysis, is described in detail. The performance of minimum variance analysis (MVA) as a wave analysis tool is investigated experimentally using this multispacecraft analysis. MVA estimates of propagation direction are shown to diverge from the multispacecraft estimate in the limit of linear wave polarization. Theoretical estimates of MVA error are also compared to the observations. Previously established wave properties derived from ISEE are independently tested; it is found that statistically, the waves propagate at frequencies an order of magnitude below the ion cyclotron frequency in the solar wind rest frame and have wavelengths of the order of an Earth radius. However, these statements mask the fact that there is significant variation about these average values that is physical in nature. The data are plotted in the $\omega - k$ plane and the average frequency and wave number are used to experimentally identify the "average" resonant beam speed. This beam speed is an order of magnitude greater than the local Alfvén speed in the solar wind rest frame. Furthermore, histograms of the inferred beam speed normalized to the solar wind speed are presented and compared to previously published plasma data. Finally, the spacecraft frame wave period is found to be proportional to the magnetic field strength in a manner consistent with previous analyses.

**Citation:** Eastwood, J. P., A. Balogh, E. A. Lucek, C. Mazelle, and I. Dandouras (2005), Quasi-monochromatic ULF foreshock waves as observed by the four-spacecraft Cluster mission: 1. Statistical properties, *J. Geophys. Res.*, *110*, A11219, doi:10.1029/2004JA010617.

## 1. Introduction

[2] This paper presents the results of a statistical investigation into the solar wind rest frame properties of 30 s period quasi-monochromatic ultra-low-frequency (ULF) foreshock waves, carried out using data from the multispacecraft Cluster mission [*Escoubet et al.*, 2001]. The aim of this investigation has been to characterize more precisely the intrinsic properties of these waves and to better understand how they are generated. It has also been our aim to experimentally investigate minimum variance analysis (MVA) as a wave analysis technique. This technique is widely used to analyze single and dual spacecraft wave observations but can be independently tested in the context of a four spacecraft mission such as Cluster. The data from this statistical study have also been used to investigate the nature of oblique wave propagation; the results of this study have also been submitted for publication [*Eastwood et al.*, 2005].

[3] The terrestrial foreshock may be defined as the region of space upstream of the bow shock filled with particles streaming away from the shock against the solar wind flow. Both ions and electrons stream away from the shock, where


0148-0227/05/2004JA010617

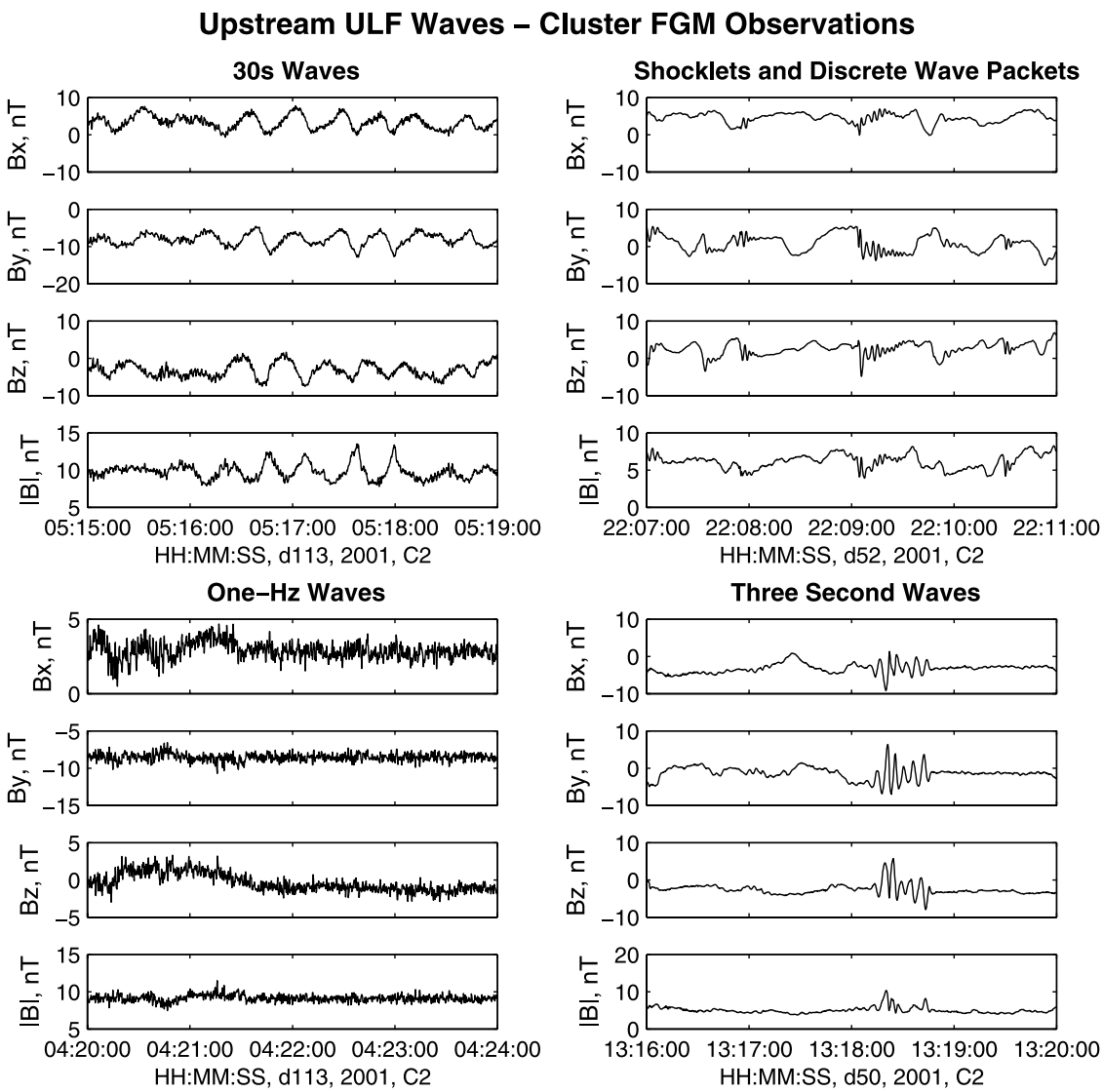


**Figure 1.** Different types of low-frequency waves observed in the foreshock.

they are subject to $\mathbf{E} \times \mathbf{B}$ drift in the solar wind; the electrons, thanks to their smaller mass, are able to escape faster upstream along the field, so the upstream boundary of the foreshock is defined by the electrons (assuming the magnetic field is not aligned to the flow) [*Fitzenreiter*, 1995]. However, in this paper, we are interested in ion driven processes. Observations of energetic ions streaming from the vicinity of the shock were first reported by *Asbridge et al.* [1968]. In fact, subsequent observations have shown that qualitatively, there are several different types of backstreaming ion distribution (e.g., reviews by *Fuselier* [1994, 1995]). The different types of backstreaming distribution commonly referred to are field-aligned (also called reflected in earlier literature), intermediate, gyrophase bunched, gyrotropic, and diffuse.

[4] The other signature of the foreshock is the existence of a variety of wave activity, due to the interaction of the solar wind and backstreaming particles. Several different types of wave have been observed in the foreshock; here we discuss only those waves related to backstreaming ions. With reference to Figure 2 of *Le and Russell* [1994], we show in Figure 1 the different lower-frequency waves that are understood to exist in the foreshock. These observations are taken from the Cluster magnetic field data set, the details of which are discussed in section 2. The top left panel shows an example of 30 s quasi-monochromatic ultra-low-frequency (ULF) waves, the top right panel shows an example of shocklets and discrete wave packets, the bottom left panel shows an example of 1 Hz waves, and the bottom right panel shows an example of 3 s waves. References to these wave types can be found in the reviews by *Le and Russell* [1994], *Greenstadt et al.* [1995], and *Burgess* [1997]. Field-aligned distributions are not associated with ULF wave activity [*Paschmann et al.*, 1979]; diffuse distributions are associated with shocklets and discrete wave packets, and intermediate/gyrophase bunched/gyrotropic distributions are observed in association with "30 s" waves.

[5] This paper is particularly concerned with the properties of the 30 s period quasi-monochromatic ULF waves. *Fairfield* [1969] demonstrated that these waves are quasi-sinusoidal, compressive perturbations in the dc magnetic field time series. In the spacecraft frame of reference, they

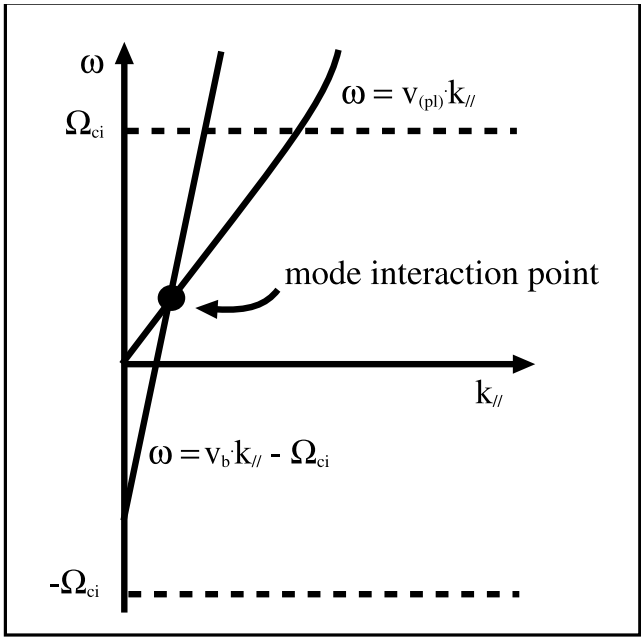


**Figure 2.** Generation of waves by cyclotron resonance shown in the $\omega - k_{\|}$ plane. The line intersecting the origin represents the dispersion relation of the fast magnetosonic wave (in the MHD approximation). At frequencies below $\Omega_{ci}$ it may be approximated as a straight line with slope $V_A$. The straight line intersecting the $\omega$ axis at $-\Omega_{ci}$ represents the beam resonance condition. At the point where the two lines cross, the growth rate is maximized. Consequently, it is expected that the waves are generated in the first instance at a localized point in the $\omega - \mathbf{k}$ plane.

have periods of the order of 30 s and are predominantly left-handed. They are often elliptically/circularly polarized [*Le and Russell*, 1994; *Burgess*, 1997]. They were initially associated with intermediate distributions, but observations of the velocity space distributions suggest that the accompanying ion distributions are often gyrophase bunched or gyrotropic rather than intermediate [*Fuselier et al.*, 1986a, 1986b; *Fazakerley et al.*, 1995; *Meziane and d'Uston*, 1998; *Meziane et al.*, 2001; *Mazelle et al.*, 2003]. To understand the source of these waves, their intrinsic properties; i.e., their properties in the solar wind rest frame must first be established.

[6] Single spacecraft data can be used to find the spacecraft frame frequency and also the direction of wave propagation (albeit with a 180° ambiguity) through the use of minimum variance analysis (MVA). The use of MVA places certain constraints on the wave polarization; this is discussed in section 3. However, neither the spacecraft frame wave speed nor the wavelength can be found. To achieve this, more than one spacecraft is required. If two spacecraft are used, the time delay between the observations of phase fronts can be used in combination with the spacecraft separation vector and MVA to find the phase speed in the spacecraft frame. Knowledge of the solar wind velocity allows the Doppler shift to be calculated, and the properties of the wave in the solar wind rest frame can then be found. If the spacecraft are separated perpendicular to the phase front, the method fails; there is no delay between the two time series, and the phase speed cannot be found.

[7] *Hoppe and Russell* [1983] applied this technique to ISEE 1 and 2 observations of foreshock wave activity. Although they were able to identify a large set of observations in the ISEE data set (121 5 min intervals of "relatively sinusoidal" ULF waves and 60 hours of "fully developed" wave activity), for reasons of geometry and wave definition, they were only able to analyze three case studies, two based on relatively sinusoidal waves and one based on fully developed waves. These case studies were sufficient to show that the waves were attempting to propagate away from the shock. Hoppe and Russell stated that the waves had "frequencies of the order of $0.1\Omega_{ci}$ and wavelengths $\sim 1\ R_E$." They did not characterize the intrinsic properties more precisely, nor did they examine any changes with solar wind conditions. Since the "30 s" waves were observed as left-handed, they were in fact right-handed and therefore consistent with generation by backstreaming ions [*Barnes*, 1970] through the right-hand resonant ion-ion beam instability [*Gary*, 1993] which would generate right-handed fast magnetosonic waves [*Krauss-Varban et al.*, 1994]. Equation (1) shows the resonance condition corresponding to the right-handed mode. The wave properties are principally controlled by the beam speed; other beam parameters control the growth rate of the instability.

$$\omega = v_b k_{\|} - \Omega_{ci} \tag{1}$$

Here, $v_b$ is the beam speed and $\Omega_{ci}$ is the ion cyclotron frequency. In Figure 2, a sketch of the beam resonance condition in the $\omega - k_{\|}$ plane is shown, together with the dispersion relation $\omega = v_{(pl)}k_{\|}$ for the fast magnetosonic branch in kinetic theory. Although the phase speed of this branch increases as the frequency approaches $\Omega_{ci}$, we are interested in low frequencies, an order of magnitude below $\Omega_{ci}$, and in the first instance the dispersion relation can be approximated to a straight line. The growth rate is maximized where the beam resonance condition crosses the dispersion relation [e.g., *Brinca*, 1991; *Gary*, 1993]. The real dispersion relation, which is modified by the existence of the beam and the thermal properties of plasma, is of course significantly more complex than a straight line.

[8] It was thought that the field-aligned (termed reflected) distributions were responsible for the generation of these waves [e.g., *Hoppe and Russell*, 1982]. The first observations of backstreaming ions prompted *Sonnerup* [1969] to propose that these ions were reflected at the bow shock. He calculated that ion reflection at the shock would lead to the production of beams with energies comparable to that of field-aligned distributions. This was tested experimentally by *Paschmann et al.* [1980], who showed that the properties of field-aligned distributions agreed with Sonnerup's prediction. While there is also evidence that such ions may also result from magnetosheath leakage [e.g., *Schwartz and Burgess*, 1984], recent evidence suggests that field-aligned distributions appear to come from the same population as the gyrating ions seen the quasi-perpendicular shock front [*Möbius et al.*, 2001].

[9] *Watanabe and Terasawa* [1984] used the model of ion reflection together with the beam generation mechanism to predict the wave properties based on the solar wind speed.

They used the solar wind speed to predict the energy of backstreaming distributions and then estimated the properties of the waves assuming that the right-hand resonant ion-ion beam instability was responsible. They again used the solar wind speed to Doppler shift the predictions, leading to a predicted spacecraft frame signature. They compared this prediction with the observed spacecraft frame wave period, finding results that were consistent with the beam generation hypothesis. Owing to their use of single spacecraft data, Watanabe and Terasawa had to make a number of assumptions in connecting together the different models, several of which are not necessary if multipoint data are available.

[10] On the basis of simulation results, it was suggested that the waves generated by the field-aligned distribution would phase trap the beam into a gyrophase bunched distribution [*Hoshino and Terasawa*, 1985]. Alternatively, the beam may also scatter into an intermediate type distribution [*Fuselier*, 1995]. However, another source of gyrophase bunched and intermediate distributions may be the shock itself. At the quasi-parallel shock, beams organized in gyrophase escape from the shock into the upstream region [*Gosling et al.*, 1982; *Gurgiolo et al.*, 1983], and intermediate distributions may escape directly from the magnetosheath [*Edmiston et al.*, 1982]. In their analysis of gyrating and intermediate ion distributions in the foreshock, *Fuselier et al.* [1986b] concluded that both beam disruption and shock reflection/magnetosheath leakage were responsible for the generation of gyrating and intermediate distributions. Furthermore, they noted that gyrating ion distributions sourced from reflection at the shock should disrupt, generating ULF waves and mixing in gyrophase [*Burgess and Schwartz*, 1984]. *Thomsen et al.* [1985] examined some examples of gyrating ions observed in conjunction with ULF waves, finding one example where the observed frequency agreed quite well with the Doppler-shifted resonance frequency of waves in right-hand resonance with the observed gyrating ions and suggesting that the waves were generated by the preexisting gyrating beam.

[11] Fully developed wave activity, corresponding to shocklets and discrete wave packets in the presence of diffuse distributions, was originally thought to represent the end point of the field-aligned beam instability [*Thomsen*, 1985]. However, since field-aligned distributions are essentially composed of protons, whereas diffuse distributions contain solar wind quantities of $He^{++}$, field aligned distributions "are not the major source of energetic [i.e., diffuse] ions in the foreshock" [*Fuselier*, 1995]. The source of the diffuse ions, their associated wave structures, and their connection to the field-aligned distributions remain to be completely understood.

[12] It was not until the launch of Cluster that these results could be investigated and extended. *Eastwood et al.* [2002] presented a case study of 30 s waves observed by Cluster and used new four spacecraft techniques to independently confirm the ISEE results. Eastwood et al. were also able to show the direct correlation of the density and field strength, something that was not done using ISEE, and made a preliminary test of MVA performance. *Narita et al.* [2003] examined the properties of fully developed foreshock wave activity using a different Cluster analysis technique, suited to the identification of coexisting wave modes. *Mazelle et al.* [2003] presented a case study examining a set of quasi-monochromatic waves and compared their intrinsic properties with simultaneously observed ion distributions. They found that the field-aligned distributions observed just before the onset of the waves closely matched the predicted beam properties derived from the wave observations. Furthermore, the properties of the gyrating ions observed in conjunction with the waves were found to be consistent with a coherent nonlinear wave particle interaction [*Hoshino and Terasawa*, 1985; *Mazelle et al.*, 2000]. A comparison of the intrinsic wave properties with the associate ion distributions was not performed in such detail using ISEE.

[13] Despite these results, certain questions remain. One concerns the validity of case studies. Up to now, multi-spacecraft investigations of the intrinsic properties of 30 s waves have relied on case studies. To what extent are these case studies representative? The intrinsic properties of the waves have been characterized to order of magnitude estimates, but they presumably also depend on the nature of their generation. If this is the case, then a statistical study ought to reveal variations about the average that can, for example, be interpreted in the context of a beam generation mechanism. Do the solar wind conditions control the wave properties in a manner that is consistent with the wave generation models [*Thomsen et al.*, 1985; *Mazelle et al.*, 2003] as currently understood? Are there any clues that might suggest how to develop our theories into the nonlinear regime? On a more practical level, Cluster represents the first opportunity to make an independent experimental test of the performance of MVA, relied on in single and dual spacecraft analysis.

[14] In this paper we address these questions by specifically examining on a statistical basis the intrinsic properties of the 30 s waves and examining how these properties correspond to the currently understood picture. We also evaluate on an experimental basis the performance of MVA. In section 2, the data are described, together with the analysis techniques used to determine wave properties in the solar wind rest frame. In section 3, minimum variance analysis is investigated. In section 4 the primary results of the statistical analysis are presented. This includes the wavelengths, phase speeds, and frequencies in the solar wind rest frame. In section 5, some derived results are presented examining the predicted beam speed as a function of the simultaneously measured solar wind speed and the relationship between the spacecraft frame wave frequency and the magnetic field strength, as discussed by *Hoppe and Russell* [1982]. Conclusions are presented in section 6.

## 2. Data Selection and Analysis Procedures

[15] The four Cluster spacecraft are in polar orbits and as such the orbital plane precesses around the Earth with a period of 1 year. The apogee of the orbit is located sunward of the terminator plane between November and May. Between February and early May 2001, the apogee of the Cluster orbit moved from ~1100 MLT to ~0200 MLT, and numerous observations of foreshock wave activity were made using the Cluster Flux-Gate Magnetometers (FGM) [*Balogh et al.*, 2001]. During this time, the scale size of the Cluster tetrahedron was ~600 km. The tetrahedron scale size is changed periodically; during the second dayside

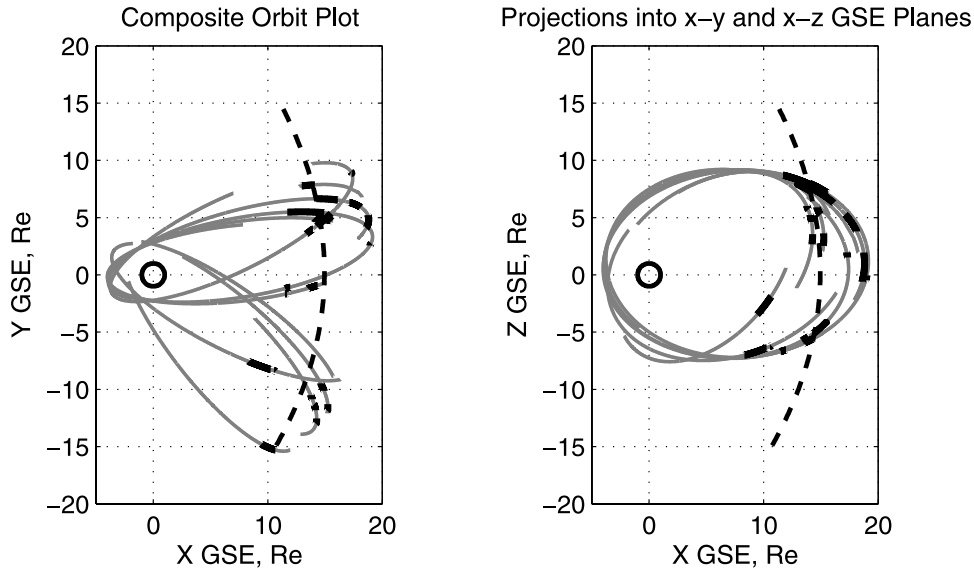


**Figure 3.** Intervals of foreshock observations forming basis of statistical analysis. The orbit is shown in gray projected into the x-y GSE plane (left) and the x-z GSE plane (right). The black dashed line represents a cut through the surface of a nominal bow shock in these planes. The sections of the orbit emboldened in black represent intervals of analyzed foreshock wave activity.

pass, the scale size was ~100 km, and during the third dayside pass, the scale size was ~6000 km.

[16] In the foreshock, the waves are convected over the tetrahedron by the solar wind at speeds of several hundred kilometers per second. If the scale size of the tetrahedron is a few hundred kilometers, this transit time is of the order of a second. The highest typical resolution of the FGM data is 22 vectors per second [*Balogh et al.*, 2001]. The smaller the tetrahedron, the closer the transit time approaches the cadence of the vector sampling. In particular, if the tetrahedron scale size is too small, the transit time of the phase fronts from one spacecraft to another may approach the sampling rate. If the sampling rate becomes less than this transit time, the wave analysis becomes meaningless. Consequently, at small separations, the discretization of the data, and the error it introduces, cannot easily be ignored. Conversely, if the spacecraft separation is too large, and approaches the expected wavelength of the waves, as was the case in the third dayside pass, the problem of spatial aliasing arises. Put simply, if the tetrahedron is bigger than the wavelength, then one cannot be sure which wave front is which in the different time series.

[17] On the basis of an orbital period of 57 hours, on approximately 35 days during this period one might expect to encounter the foreshock. However, data acquisition was limited by the operational cycle of the spacecraft during the first year of flight in 2001, and here we present a statistical study based on foreshock observations available over 12 different days in this period. Figure 3 shows the spatial distribution of the observations. The orbit of Cluster 1 is shown on different days in gray, projected into the x-y GSE and x-z GSE planes in the left and right panels, respectively. In early February 2001 the apogee of the orbit was located just on the dusk flank of the bow shock. During the next 3 months, the orbital apogee precessed dawnward, through the expected location of the foreshock for a spiral IMF orientation. The dashed black curves correspond to cuts through a nominal bow shock surface, based on the average shape of the *Peredo et al.* [1995] bow shock model. The sections of the orbits marked in black correspond to intervals of analyzed foreshock wave activity. The observations cover a wide range of local times, magnetic field orientations, and upstream conditions.

[18] Each day contained several separate encounters with the foreshock, either due to the outbound/inbound orbital motion of the spacecraft or due to changes in the location of the foreshock in front of the bow shock, controlled by the Interplanetary Magnetic Field (IMF) orientation. The available FGM data were examined for the existence of foreshock ULF wave activity, in the presence of backstreaming ions as observed by the Cluster Ion Spectrometry (CIS) experiment [*Rème et al.*, 2001]. Intervals consisting entirely of shocklets and discrete wave packets were rejected. Thirty-one separate intervals of foreshock wave activity were retained, ranging in length from <15 min to >1 hour.

[19] In general, we found that the background IMF orientation was not very stable; discontinuities and rapid changes in magnetic field orientation were often observed. The background magnetic field strength was seen to vary, as was the plasma density and solar wind velocity. This has two consequences. The first is that if the orientation of the IMF changes, the upstream boundary of the foreshock moves. The spacecraft become connected to a different point on the shock and may find themselves in a different part of the foreshock. Consequently, an interval of apparently continuous foreshock wave activity that contains a discontinuous change in IMF for example cannot be treated as one interval. Second, the orientation of the IMF controls the direction of wave propagation to first order, and the Doppler shift depends on the orientation of the wave fronts relative to the solar wind. If the IMF is changing orientation, the Doppler shift is also presumably changing, and even if this is the "same" wave throughout, the spacecraft frame wave period may vary. Furthermore, changes in the strength

of the background magnetic field will change the ion cyclotron frequency and therefore the observed wave period.

[20] The rich variety of behavior caused us to proceed with caution. In addition to the issues described above, it was found that the intervals of continuous wave activity selected for further analysis were not homogenous in nature. The amplitude and phase profile of the waves were observed to vary on timescales of minutes. Discrete wave packets were occasionally observed to appear for one or two wave cycles. At 600 km separation, many of these changes were correlated between the spacecraft and in general, the same large-scale, nonlinear wave profile would be seen in each of the time series. Nevertheless, the waves would also occasionally become decorrelated, particularly at higher frequencies, or would become so ill-defined that a repeating wave profile was not observed.

[21] Since we are interested in the properties of a single wave mode that is steepening and therefore quasi-monochromatic, and whose properties may be time dependent, it was decided to proceed with the previously developed cross-correlation timing analysis [*Eastwood et al.*, 2002, 2004] rather than k-filtering or similar wave telescope techniques [*Pinçon and Motschmann*, 1998; *Narita et al.*, 2003; *Eastwood et al.*, 2004]. The usefulness of array wave analysis techniques lies in their ability to identify multiple coexisting wave modes, which is not required here. Also, the use of array wave analysis techniques places certain constraints on the data; in particular the wave activity should be homogenous and the background plasma parameters should be constant. It should be noted that wave array techniques result in an interpretation that implies a superposition of waves is present when a steepened nonlinear wave is observed. Then analyzing the dominant frequency component is somewhat debatable, although if the waves are nondispersive in the frequency regime of interest, this should not matter. Given the variability of the data, described in the previous paragraph, and for reasons of computational efficiency, the cross-correlation technique was felt to be more appropriate. The cross-correlation timing analysis technique looks for the phase lags between the spacecraft time series and simply requires the waves profile to be similar in each time series. Implicit in this approach is the fact that the waves are being described as a single, steepened, nonlinear entity, rather than a fourier superposition of sinusoidal waves. Therefore this technique is inappropriate when multiple waves coexist, for example in the magnetosheath. The technique also allows the time-dependent nature of the observations to be accessed.

[22] Each of the 31 intervals were filtered to remove any high-frequency ($\sim 10^{\circ}$ Hz) signatures (in particular any coexisting 1 Hz whistler waves) and then divided into 2 min sections. This time length was chosen on the basis of practical experience; the effects of changes in the background plasma parameters are minimized, but the interval contains several wave periods, allowing the data to be cross-correlated. In each such interval, the background plasma parameters have to be treated as constant. Each subinterval was then analyzed individually, first being rejected if any data gaps were found. Wavelet analysis [*Eriksson*, 1998] was used to ensure the concentration of wave power at one frequency and to check that the waves were left-handed in the spacecraft frame [*Means*, 1972].

[23] Minimum variance analysis (MVA) [*Song and Russell*, 1999] was used to calculate the maximum variance time series at Cluster 1. The Cluster 1 variance coordinate system was then applied to the other spacecraft magnetic field time series to produce pseudo-maximum variance time series for Cluster 2, 3, and 4. An alternative approach would have been to calculate the maximum variance time series for each spacecraft independently. However, when circularly polarized waves are observed, the intermediate and maximum variance time series can become degenerate. Consequently, the maximum variance direction at Cluster 1 may not be aligned with that of Cluster 2, which leads to the introduction of artificial phase differences when comparing the two maximum variance time series.

[24] The autocorrelation of each (pseudo)-maximum variance time series was then calculated [*Bendat and Piersol*, 1986]. If no second maximum in the autocorrelation was observed, at any spacecraft, or if the autocorrelation did not smoothly vary, the interval was rejected. The average autocorrelation was used to calculate the period of the wave in the spacecraft frame. The time series were then cross-correlated [*Bendat and Piersol*, 1986]. The cross-correlations center on the largest repeating feature in the time series, the wave of interest, and give the time differences between spacecraft observations of the phase fronts. If the cross-correlation between any spacecraft pair was less than 0.8, the interval was rejected on the basis that the different magnetic field time series were not sufficiently well correlated. The time differences were then used to find the wave k vector and the phase speed, based on a timing analysis [*Schwartz*, 1998]. The method assumes that the waves are planar on the scale of the spacecraft separation and that they are moving at constant speed in the spacecraft frame. Both conditions are expected to be well met.

[25] This calculation resulted in the speed and direction of propagation in the spacecraft frame. This was then combined with the measurement of the spacecraft frame frequency from the autocorrelation to calculate the wavelength of the waves, which is frame-independent. Finally, measurements of the solar wind speed from Cluster CIS-HIA [*Rème et al.*, 2001] on Cluster 1 were used to construct the Doppler shift, converting the results from the spacecraft frame into the solar wind rest frame and giving the propagation speed in the solar wind rest frame. Intervals of wave activity where suitable solar wind data were not available were not included in this analysis. Since the direction of propagation and wavelength is frame-independent, this allowed the frequency in the solar wind rest frame to be calculated. This procedure resulted in a sample of 255 2-min observations of quasi-monochromatic ULF wave activity, covering a range of upstream conditions.

## 3. A Statistical Test of Minimum Variance Analysis

[26] The principal technique used in single and dual spacecraft analysis of waves in magnetic field time series is minimum variance analysis (MVA) [e.g., *Sonnerup and Scheible*, 1998; *Song and Russell*, 1999]. MVA uses a time series of data, typically the magnetic field, to estimate the normal orientation of a one-dimensional current sheet or

wave front in a plasma. The method finds a coordinate system [$\mathbf{x}_1$ $\mathbf{x}_2$ $\mathbf{x}_3$] to describe the data such that the variance in $\mathbf{B}.\mathbf{x}_3$ is minimized and the variance in $\mathbf{B}.\mathbf{x}_1$ is maximized. [$\mathbf{x}_1$ $\mathbf{x}_2$ $\mathbf{x}_3$] are referred to as the maximum, intermediate and minimum variance directions respectively. Associated with [$\mathbf{x}_1$ $\mathbf{x}_2$ $\mathbf{x}_3$] are the eigenvalues $\lambda_1$, $\lambda_2$ and $\lambda_3$, which represent the variance of the magnetic field along the different directions ($\lambda_1 \geq \lambda_2 \geq \lambda_3$).

[27] Across a one-dimensional current sheet, the normal component of the magnetic field is constant, and so the variation in **B** is minimized. Therefore by applying MVA to a time series of the crossing, we can calculate the direction of minimum variance and identify this as the direction of the normal. However, if the magnetic field perturbation is linearly polarized, the variation in the field is confined to a single direction. Although the maximum variance direction is well defined ($\lambda_1$ is large) $\lambda_2 \approx \lambda_3$, and the intermediate and minimum variance directions are degenerate. The normal cannot, with confidence, be identified as the minimum variance direction. For example, at a shock, the magnetic field upstream and downstream magnetic fields are coplanar. Since the normal component of the magnetic field is conserved, the field strength changes only in the transverse direction; this perturbation is linearly polarized, and MVA cannot be used [e.g., *Schwartz*, 1998].

[28] MVA can also be applied to the analysis of waves; here the minimum variance direction can be identified as the direction of wave propagation. There is a 180° ambiguity, since it is not possible to say in which direction the wave is propagating. The same caveat concerning polarization applies; if the waves are linearly polarized, then the intermediate and minimum variance directions are degenerate, and the orientation of the wave normal cannot be confidently found.

[29] Since MVA is such a widely used technique and lies at the heart of both single and dual spacecraft wave analysis, efforts have been made to understand errors and the problem of degeneracy [e.g., *Sonnerup and Scheible*, 1998, and references therein]. The statistical error in the minimum variance direction depends on $N^{-1/2}$, where N is the size of the data set, and on $\lambda_2$ and $\lambda_3$, as shown in equation (2) [e.g., *Mazelle et al.*, 2003]. Sonnerup and Scheible proposed that $\lambda_2/\lambda_3 > 10$ as starting point when the data set is small (N = 50).

$$\Delta\theta_{kB} = \sqrt{\frac{\lambda_3}{(N-1)}\frac{\lambda_3}{(\lambda_2-\lambda_2)^2}} \qquad (2)$$

Here we can assess the performance of MVA in a new way by comparing it with the results of the multispacecraft analysis. For each 2 min interval of wave activity, MVA was applied to each of the four spacecraft time series. The minimum variance direction $\mathbf{x}_3$ and the ratio of intermediate to maximum eigenvalues $\lambda_2/\lambda_3$ were calculated for each spacecraft and then averaged. Although high-resolution data (22 vector/s) were used (each interval containing more than 2600 samples) the data were filtered, and the loss of information corresponds to an effective reduction in the number of samples. The cross-correlation timing analysis was then used to estimate the direction of wave propagation independently of MVA for the same interval. $\Delta\theta$, the angle between the average MVA minimum variance direction and the four spacecraft estimate of the phase front orientation was then calculated. This angle was forced to lie between 0 and 90°, which is allowed since the minimum variance direction may be parallel or antiparallel to the propagation direction.

[30] The results of this analysis are shown in Figure 4, where $\Delta\theta$ is plotted as a function of $\lambda_2/\lambda_3$. Here $\Delta\theta$ becomes small as $\lambda_2/\lambda_3$ increases, but as $\lambda_2/\lambda_3$ approaches 1, $\Delta\theta$ on average increases. The gray line in Figure 4 shows the theoretical error in the MVA estimate of the propagation direction based on equation (2). The error in the four spacecraft estimate is of the order of a few degrees, independent of the eigenvalue ratios. As $\lambda_2/\lambda_3$ approaches 1, the wave becomes linearly polarized and the error in the MVA direction rapidly increases. If $\lambda_2/\lambda_3 \gg 1$, the wave is not linearly polarized, and the error in the minimum variance direction converges to 0. It should be pointed out that even if $\lambda_2/\lambda_3$ is large, the wave may still be highly elliptical, if $\lambda_1/\lambda_2$ is also large. However, MVA simply requires that the minimum variance direction is well defined.

[31] Figure 4 therefore shows experimentally that the MVA estimate of the wave propagation direction approaches the four spacecraft estimate in the regime where it is theoretically expected to perform well. The fact that the difference between the two estimates is a little larger than one might expect from the errors in the two estimates when $\lambda_2/\lambda_3$ is small may suggest that the error estimates are perhaps conservative. *Sonnerup and Scheible* [1998] note that in the limit of linear polarization, the linear theory used to compute the theoretical MVA error breaks down. This experimental test of MVA is in broad agreement with theoretical treatments of MVA error [e.g., *Sonnerup and Scheible*, 1998]. In particular, the basic rule of using MVA in small data sets when $\lambda_2/\lambda_3 > 10$ is reflected in our data here (recalling that the filtering of the data has effectively reduced the number of sample points). Experimentally, if $\lambda_2/\lambda_3 < 5$, MVA apparently cannot be used to reliably determine the orientation of phase fronts. A preliminary case study of MVA performance is also seen to be consistent with these results [*Eastwood et al.*, 2002].

## 4. Primary Results of the Statistical Analysis

[32] In this section we present the primary results of the statistical analysis, which relate to the intrinsic properties of the observed waves. The left-hand panel of Figure 5 shows a histogram of the spacecraft frame wave periods, $f_{(s/c)}$. The majority of the observations lie in the 25 s, 30 s, and 35 s period bins, and the mean value is 31 s. However, waves with both longer and shorter spacecraft frame period were observed. The error in any individual observation is of the order of 1 s, or 5%. Therefore the spread corresponds to real variability. The right-hand panel of Figure 5 shows the same data, scaled to the local ion cyclotron frequency, $\Omega_{ci}$. Even though the data are now scaled, there is still significant variation. This variation is presumably related to the way in which the waves are generated, through differences in the initial conditions (geometry and beam speed) and/or through differences in the nonlinear evolution of the insta-

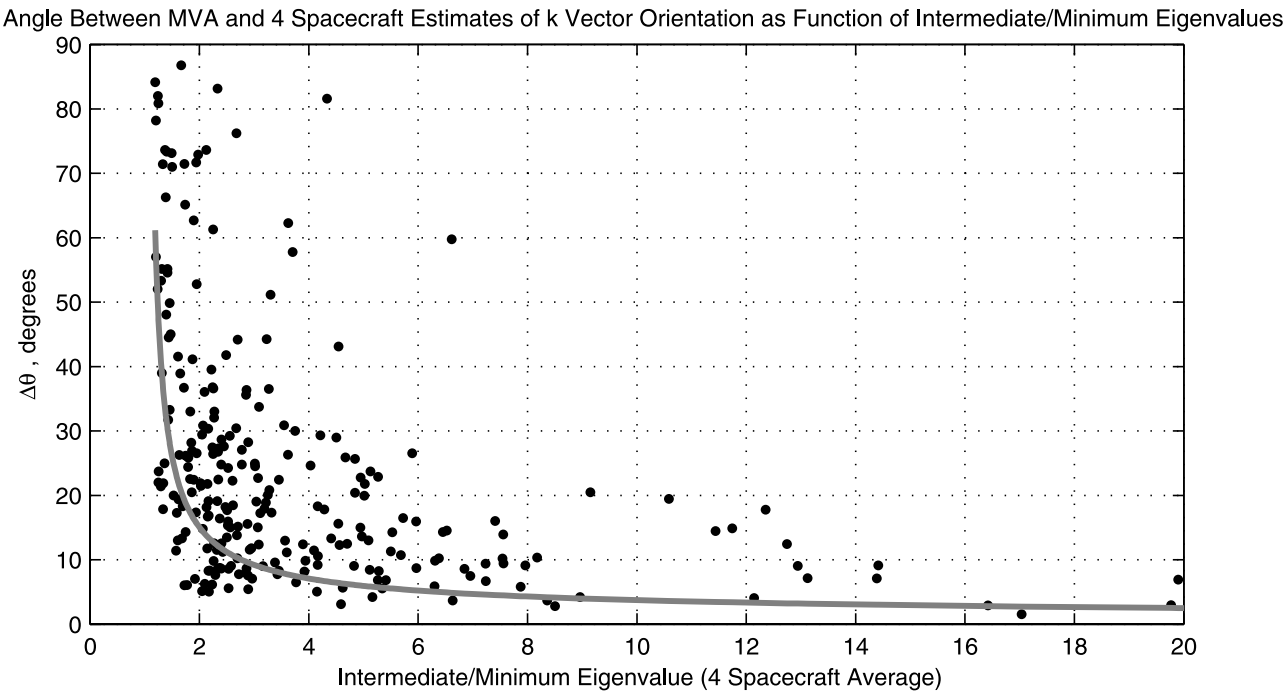


**Figure 4.** Angle between MVA minimum variance direction and four spacecraft estimate of the phase front orientation, as a function of intermediate/minimum eigenvalues. The MVA results are averaged over the four spacecraft. The gray line shows the theoretical error in the MVA estimate. The error in the four spacecraft estimate is of the order of a few degrees, independent of $\lambda_2/\lambda_3$.

bility. Before examining this in more detail, we consider the wavelengths.

[33] The left-hand panel of Figure 6 shows a histogram of the observed wavelengths $\lambda$, where $\lambda = v_{(s/c)}/f_{(s/c)}$. The timing analysis gives the spacecraft frame phase speed $v_{(s/c)}$. The mode of the distribution is 1 $R_E$ and the mean is 1.5 ±.0.7 $R_E$. This is consistent with *Hoppe and Russell*'s [1983] statement that the wavelength is ~1 $R_E$. The experimental error in $v_{(s/c)}$ is of the order of 5%, and so the experimental error in individual measurements of $\lambda$ is 5–10%. The spread in $\lambda$ about the average therefore corresponds to real variability in the wavelength. The waves are propagating obliquely to the magnetic field, with the average $\theta_{kB} = 21°$. The right-hand panel of Figure 6 shows a histogram of the wave numbers,

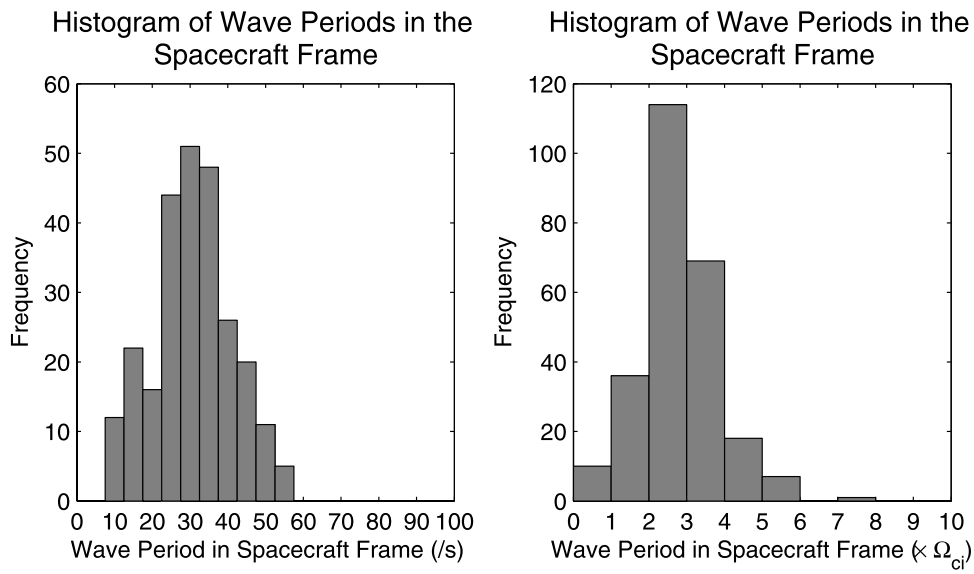


**Figure 5.** Histogram of wave periods observed in the spacecraft frame over 255 samples. The waves are quasi-monochromatic in the individual cases. The left-hand panel shows the raw data. The variation about the average is significantly larger than the experimental error in each observation. The right-hand panel is scaled to the local proton gyrofrequency.

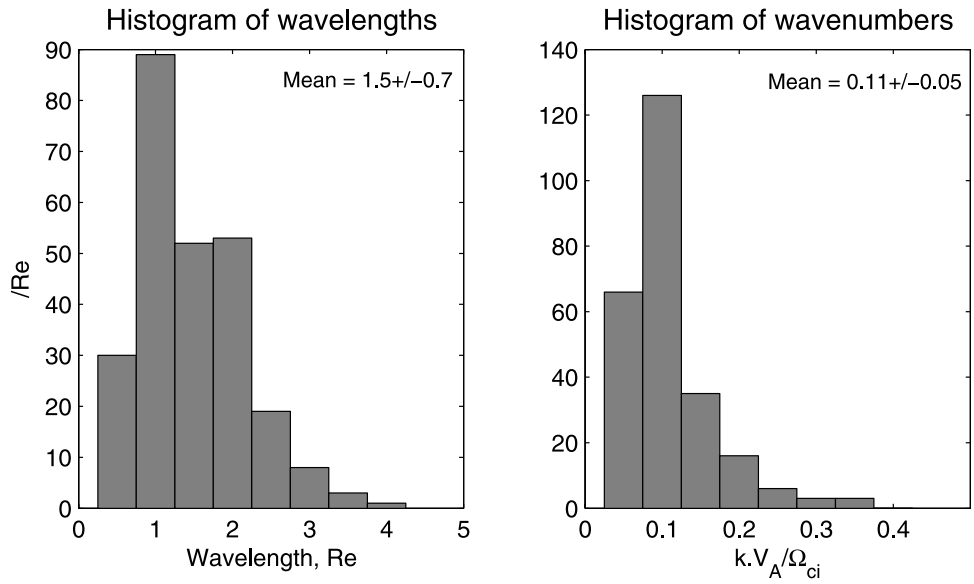


**Figure 6.** The left-hand panel shows the histogram of wavelengths, calculated from the four spacecraft timing analysis. The mode is the 1 $R_E$ bin. The right-hand panel shows the histogram of wave numbers, scaled to units of $\Omega_{ci}/V_A$.

scaled to $\Omega_{ci}/V_A$. Again, even though the data are scaled, there is still significant variation. As with the frequencies, this variation is due to some extent to the initial conditions and/or also to the nonlinear evolution of the instability.

[34] To investigate this further, we examined the properties of the waves in the solar wind rest frame. To do this, a frame transformation must be applied based on the solar wind velocity. This gives the phase speed in the solar wind rest frame $v_{(pl)}$ where

$$v_{(pl)} = v_{(s/c)} - \mathbf{v}_{sw} \cdot \hat{\mathbf{k}} \tag{3}$$

$\mathbf{v}_{sw}$ is the solar wind velocity, and $\hat{\mathbf{k}}$ is the unit k vector. Given the uncertainty in the solar wind velocity (a few percent), the error in the orientation of the k vector and the error in the spacecraft frame phase speed, the experimental error in $v_{(pl)}$ is of the order of 20–40%. For each of the 255 intervals of quasi-monochromatic ULF wave activity, the wave speed in the solar wind rest frame was calculated, normalized to the local Alfvén speed. The Alfvén speed rather than the sound speed was used because of its importance in kinetic wave theory [*Krauss-Varban et al.*, 1994]. The average phase speed was found to be $v_{(pl)} = 1 \pm 0.6V_A$ directed sunward (i.e., $k_x > 0$), where the error is the standard deviation. A significant component of this error can be accounted for by experimental uncertainties, and we may conclude that the waves are propagating upstream and that the propagation speed is of the correct order of magnitude. The dependence of the wave speed on the actual numerical value of the Alfvén speed was also investigated. Although some evidence was found suggesting that the wave speed tended to drop below the Alfvén speed as the Alfvén speed increased, the result was not statistically certain and is not discussed in further detail here.

[35] Since the wavelength $\lambda$ is frame-independent, we can also calculate $f_{(pl)} = v_{(pl)}/\lambda$. However, the experimental errors in $\lambda$ and $v_{(pl)}$ are ~7% and ~20–40%, respectively, leading to an experimental uncertainty in $f_{(pl)}$ of again ~40%. This is comparable to the variation in $\Omega_{ci}$ (which is controlled by the magnetic field strength). *Hoppe and Russell* [1983] concluded from ISEE observations that "[the waves] center about frequencies of the order of $0.1\Omega_{ci}$." We find that $\omega_{pl} = 0.10 \pm 0.08\ \Omega_{ci}$. The range of $\Omega_{ci}$ was from 0.30 to 1.82 $s^{-1}$. We attempted to investigate whether this relationship held as $\Omega_{ci}$ varied by calculating $r_c$, Spearman's ranked correlation coefficient [e.g., *Devore*, 2000]. This statistic ranks the data in each data set according to their numerical values and then computes the correlation between the two rankings. The use of rank rather than absolute numerical values reduces the effect of outlying points. The random variable $r_s$ follows the t distribution with N-2 degrees of freedom and can be used to test the hypothesis $H_0$ that there is no correlation between the two parameters ($r_s = 0$) against the hypothesis $H_1$ that the two parameters are correlated ($r_s \neq 0$). The test statistic t is given by equation (4):

$$t = r_s \sqrt{\frac{N-2}{1-r_s^2}} \tag{4}$$

Here, $r_s = 0.367$, $N = 255$, and $t = 6.267$. At the 99% significance level, $t_{crit} = 2.576$; hence the hypothesis $H_0$ is rejected, and the hypothesis $H_1$ is accepted; the correlation is significant at the 99% level. However, although the correlation is significant, we were unable to ascertain the exact way in which $f_{(pl)}$ depends on $\Omega_{ci}$ because the experimental uncertainty in $f_{(pl)}$ dominated.

[36] To conclude the results of this section: the average spacecraft frame period was 31 s, but variability of more than ±10 s was observed, greatly exceeding the experimental error associated with individual measurements. Typical wavelengths were of the order of 1 $R_E$, but again significant variability greater than the experimental error was seen. These variations are therefore physical and related to the

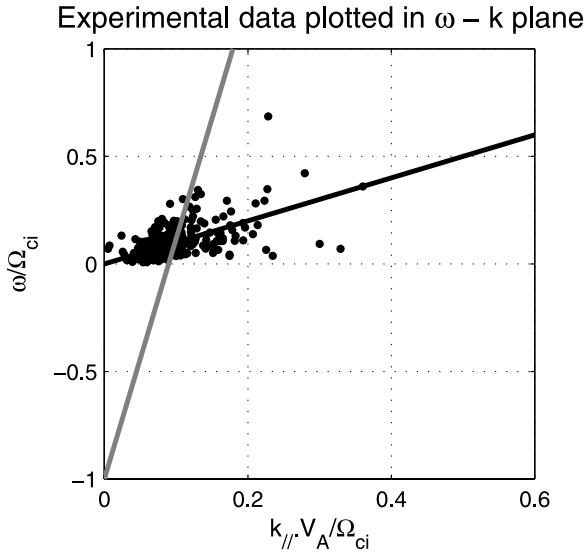


**Figure 7.** Plot of plasma frame wave frequency normalized by $\Omega_{ci}$ against parallel wave number, normalized by $\Omega_{ci}/V_A$, for each of 255 subintervals of monochromatic ULF wave activity. The experimental error in $\Omega_{ci}/V_A$ is ~20–40%. The black line corresponds to the Alfvèn speed. Clustering of the data is seen, as might be expected from Figure 2. The gray line, based on the mean values of frequency and wave number, represents the beam resonance condition.

"initial" conditions (e.g., beam speed, foreshock geometry), and/or the nonlinear evolution of the instability. The plasma frame wave speed was found to be of the order of the local Alfvén speed, with the waves propagating sunward in the solar wind rest frame. The average plasma frame wave frequency was $0.1\Omega_{ci}$. A larger error in both the plasma frame wave speed and frequency is introduced by the Doppler shift. The plasma frame frequency and $\Omega_{ci}$ are correlated statistically, but any linear regression is concealed by the experimental error. In the next section, the cause of the underlying physical variation in $f_{(s/c)}$ and $\lambda$ is considered.

## 5. Results Derived From the Primary Analysis

[37] Since these waves are principally left handed in the spacecraft frame, the fact that they are attempting to propagate sunwards means that the solar wind Doppler shift induces a reversal in the observed polarization. They are therefore intrinsically right-handed, suggesting that these waves lie on the fast magnetosonic branch of the kinetic dispersion relation.

[38] In section 4, it was shown that there was significant real variability in both the spacecraft frame wave period and the wavelength. This variability is directly related to their generation and may depend on the "initial" conditions such as the speed of the beam or on the nonlinear evolution of the beam instability itself. To understand this better, a first step can be made by considering the beam resonance condition, shown in equation (1). It is instructive to see how the experimental data appear when plotted in the $\omega - k_{\|}$ plane. For each subinterval, the plasma frame wave frequency, normalized by $\Omega_{ci}$, and $k_{\|}$, normalized by $\Omega_{ci}/V_A$, were calculated. These parameters were then plotted against each other, shown in Figure 7. The experimental error in each frequency is of the order of 30%, and in each wave number is of the order of 10%. It is important to note that this is not an attempt to derive the dispersion relation per se as with the k-filtering technique. If there were significant wave activity over a broad frequency range in a single interval, then one could determine the energy peak in k space over a range of frequencies and plot the resulting dispersion relation directly. Here the entire dispersion relation cannot be mapped by using k-filtering because there is no significant wave activity and therefore no power through the majority of the frequency range (other than the fluctuations associated with background solar wind turbulence).

[39] We expect the points to be clustered where the growth rate is maximized, as shown in Figure 2. The data are clustered, but the existence of experimental errors and the fact that for each point, the underlying plasma conditions (e.g., the beam speed) may have been different must be borne in mind.

[40] The mean frequency and wave number were found to be $0.11\Omega_{ci}/V_A$ and $0.10\Omega_{ci}$ respectively. These data were used in equation (1) to calculate an "average" beam speed, which is plotted as a gray line in Figure 7. This line intersects the frequency axis at $-1\Omega_{ci}$ and its gradient is $10.1V_A$. Experimentally, this result implies that the beam speed is typically an order of magnitude greater than the Alfvén speed in the solar wind rest frame. The black line in Figure 7 corresponds to the Alfvén speed. For frequencies well below $\Omega_{ci}$, kinetic theory shows that these waves propagate at speeds of the order of the Alfvén speed, although the presence of the beam will modify the phase speed somewhat [*Krauss-Varban et al.*, 1994]. The average phase speed is consistent with propagation at the local wave speed, and the data are statistically correlated (Spearman's rank correlation coefficient was calculated from the frequency and wave number data, giving $r_s = 0.565$; this is significant at the 99% level where the test statistic $t = 10.9$ compares to $t_{crit} = 2.576$).

[41] The properties of backstreaming ion distributions have been investigated by a number of authors. *Bonifazi and Moreno* [1981] used ISEE data to establish the properties of reflected, intermediate, and diffuse ions in the spacecraft frame. They found that typically $v_b/v_{sw}$ ~2 for reflected (i.e., field-aligned) distributions, ~1.7 for intermediate and ~1.2 for diffuse where $v_b/v_{sw}$ is the normalized guiding center speed in the spacecraft frame. Table 1 of *Hoppe and Russell* [1982] indicates that for field-aligned distributions, $v_b/v_{sw} = 2.5 \pm 0.3$, as derived from plasma measurements. This corresponds to the beam speed parallel to the field relative to the parallel component of the solar wind velocity. More recently, *Meziane et al.* [2004] have identified an example of a field-aligned beam with $v_b/v_{sw} = 1.68$, and a backstreaming gyrating ion beam with $v_b/v_{sw} = 1.52$.

[42] To compare our data with these plasma observations, equation (1) was used to infer the beam speed $v_b$ for each interval of wave activity. These data are shown in Figure 8. The top left panel shows a histogram of the inferred beam speed in the solar wind rest frame, normalized to the simultaneously observed solar wind speed. It was found

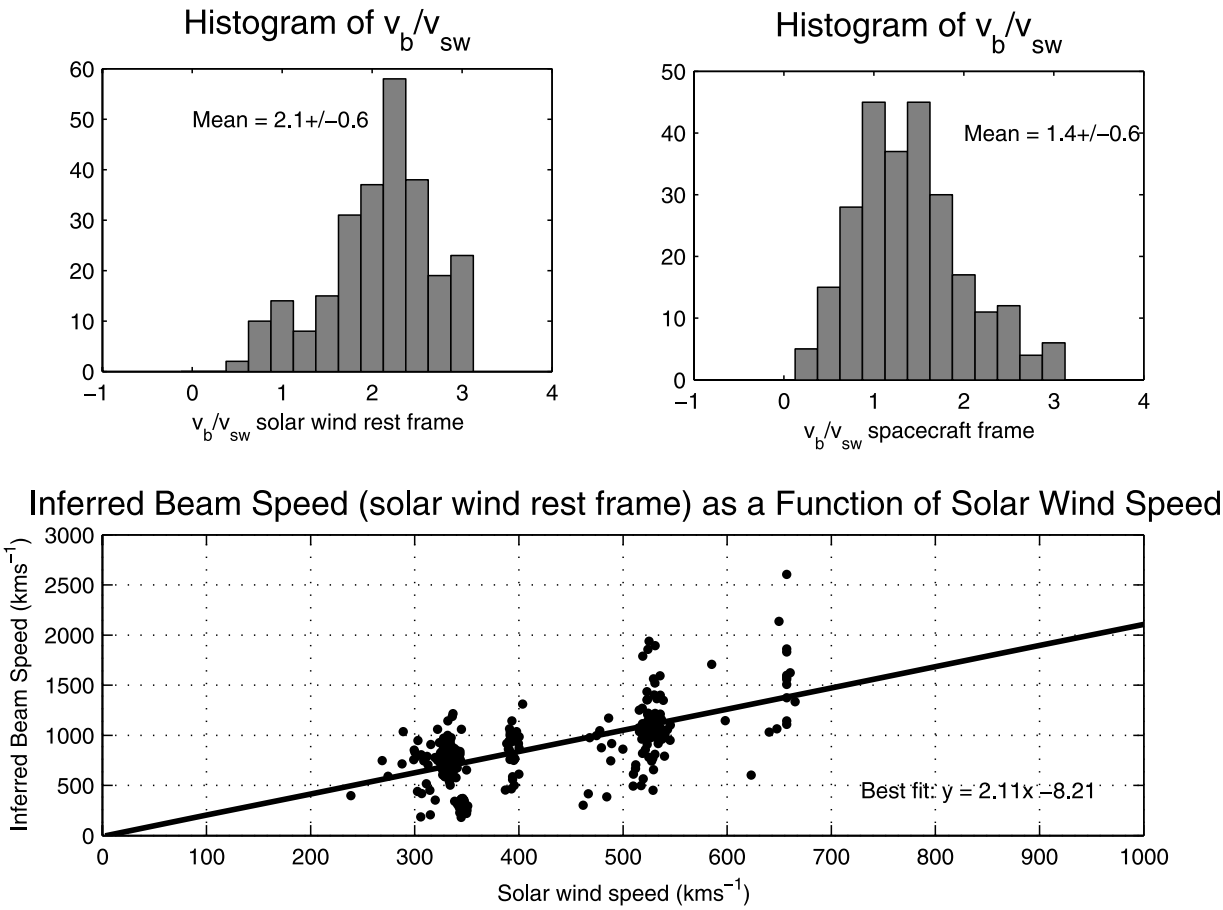


**Figure 8.** The two histograms show the beam speeds inferred from the wave observations as a function of solar wind speed. The left-hand histogram is based on the beam speed in the solar wind rest frame. The right-hand histogram is based on the beam speed in the spacecraft frame (the guiding center speed), for direct comparison with the statistics of *Bonifazi and Moreno* [1981]. The bottom panel shows the beam speed, inferred from the wave properties, in the solar wind rest frame as a function of solar wind speed. The black line represents the linear regression and has a slope of 2.11.

that in the solar wind rest frame, $v_b/v_{sw} = 2.1 \pm 0.6$. The top right panel shows another histogram of $v_b/v_{sw}$ in the spacecraft frame (normalized guiding center speed). In this frame, $v_b/v_{sw} = 1.4 \pm 0.6$. Comparing the histogram of inferred beam speeds in the spacecraft frame with the results of *Bonifazi and Moreno* [1981] (particularly Figure 4 therein), it can be seen that whilst some of these waves are highly likely to arise from field-aligned distributions (particularly where $v_b/v_{sw} > 2$), other waves result from slower beams consistent with intermediate or even diffuse distributions. However, as pointed out by Bonifazi and Moreno, the ratio $v_b/v_{sw}$ is to be used carefully.

[43] In the bottom panel of Figure 8 the inferred beam speed in the solar wind rest frame is plotted as a function of the simultaneously measured solar wind speed. The linear regression, shown in black, is $2.11 \pm 0.32$ at the 95% significance level. Note that although the average beam speed increases with solar wind speed (bottom panel), and although the data are correlated (Spearman's rank correlation coefficient $r_s = 0.58$ for these data. The test statistic for the correlation is $t = 11.47$, which is significant even at the 99.9% level where $t_{crit} = 3.291$), the coefficient of determination = 0.4. This coefficient measures the extent to which the linear regression explains the observed data (a coefficient of 1 means that the regression is perfect) [e.g., *Devore*, 2000].

[44] Therefore although there is a correlation between the beam speed and the solar wind speed, there is significant variation in the inferred beam speed for any particular solar wind speed. This is accounted for in part by the experimental error, which is ~10%. A second effect is due to the geometry of foreshock; as stated above, the actual beam speed is a function of shock geometry. Incorporating a model of the beam production process that accounts for both the shock geometry and the reflection or leakage mechanism may help to further understand the observed variability in $v_b/v_{sw}$.

[45] Finally, on the basis of observations at Mercury, Venus, Earth, and Jupiter, *Hoppe and Russell* [1982] established that the wave frequency in the spacecraft frame was linearly correlated with the upstream magnetic field strength by a factor of 0.006 for $0.1 < B < 50$ nT. This was interpreted in terms of cyclotron resonance conditions, drawing together different equations to link these two parameters. In this data set, the mean magnetic field was found to be 6.3 nT and the mean wave frequency 0.032 Hz;

i.e., f = 0.005B, consistent with the results of *Hoppe and Russell* [1982].

[46] To summarize the results of this section: the mean wave number and frequency were found to be $0.11\Omega_{ci}/V_A$ and $0.10\Omega_{ci}$. Using equation (1), this corresponds to a mean beam speed of $10.1V_A$. The inferred beam speed as a function of simultaneously measured solar wind speed was also calculated. In the solar wind rest frame, $v_b/v_{sw} = 2.1 \pm 0.6$ and in the spacecraft frame, $v_b/v_{sw} = 1.4 \pm 0.8$. Finally, the spacecraft frame frequency of the waves was found to be proportional to the magnetic field strength in a manner consistent with previous observations.

## 6. Discussion and Conclusions

[47] In this paper we have examined the statistical properties of a particular type of foreshock wave, the quasi-monochromatic ULF wave. Previously published experimental and theoretical evidence has established that these waves are generated by the interaction between backstreaming ion distributions and the inflowing solar wind through the right hand ion-ion cyclotron beam instability. Previous multispacecraft analysis of these waves from both ISEE and Cluster has concentrated on case studies. Here, we have used data from Cluster to study on a statistical basis the intrinsic properties of these waves. Cluster is not constrained by the geometrical limitations of dual spacecraft analysis, nor is it restricted by the caveats associated with minimum variance analysis. The Cluster analysis allows the solar wind rest frame properties of the waves to be calculated with fewer assumptions and allows the properties of the waves to be found more accurately.

[48] Data from the first year of Cluster observations, when the spacecraft separation was of the order of 600 km, has been used. A large set of foreshock observations were collected, and intervals of quasi-monochromatic "30 s period" foreshock ULF waves were identified. These observations were analyzed using a cross-correlation timing analysis technique, resulting in a statistical set of observations (255 2-min intervals) of "30 s" waves.

[49] The data were used to make an experimental test of the minimum variance analysis technique. MVA and the Cluster analysis technique were applied to the same data, and the results were compared. It was found that in the limit of linear wave polarization, MVA performed poorly, as expected theoretically, and that if the ratio of intermediate to minimum eigenvalues is used to characterize this, then when $\lambda_2/\lambda_3 < 5$, MVA should not be used. If $\lambda_2/\lambda_3 > 10$, then MVA can be used more reliably, in broad agreement with theoretical considerations. It should also be noted that for a large fraction of the data set, MVA cannot be used to study the orientation of wave vectors, and therefore that studies based on single and dual spacecraft observations are inherently limited.

[50] For each sample, the spacecraft frame wave period and the wavelength were calculated. The average spacecraft frame wave period was found to be 31 s, and the average wavelength (which is frame-independent) was found to be $\sim 1\ R_E$. Both quantities exhibited significant variability about the average greater than the experimental error. Fundamentally, this arises from variability in the "initial" conditions (e.g., beam speed, foreshock geometry), and/or processes associated with the nonlinear development of the wave-particle interaction.

[51] To investigate this, as a first step the wave properties in the solar wind rest frame were found. The waves propagated sunward in the solar wind rest frame, at speeds of the order of the Alfvén speed. The wave frequency was on average an order of magnitude less than $\Omega_{ci}$. On the basis of the polarization, these waves were identified as kinetic fast magnetosonic ULF waves. The introduction of the Doppler shift meant that the solar wind rest frame parameters were subject to a larger error; this meant that although a correlation between the wave frequency and $\Omega_{ci}$ could be established, linear regression could not be applied. Previous estimates have characterized the frequency and wavelength of these waves to order of magnitude statements; here we find that certainly in the case of the wavelength, there is significant physical variation about the average. An investigation into the relationship between the magnetic field strength and the spacecraft frame wave period found results consistent with previously analyses. Observations of other planetary foreshocks (e.g., by Cassini at Saturn) will allow the range of parameter space over which this relationship can be investigated to be extended.

[52] The waves are thought to be generated by backstreaming ion distributions through the right-hand resonant ion-ion beam instability, summarized by equation (1). The data were plotted in the $\omega - k$ plane, and the average frequency and wave number were used to compute an "average" beam speed, found to be an order of magnitude greater than the Alfven speed. However, this did not account for differences in the plasma properties between individual observations. The spread in wave number was greater than the error in individual observations suggesting that a range of beam speeds were responsible for the different wave observations.

[53] To further investigate this, each wave observation was used with the resonance condition (equation (1)) to compute an inferred beam speed. The average inferred beam speed, normalized to the solar wind speed, was found to be $1.4 \pm 0.6$. This result may be compared with the statistical properties of backstreaming distributions presented by *Bonifazi and Moreno* [1981] and *Hoppe and Russell* [1982]. Bonifazi and Moreno found that $v_b/v_{sw} \sim 2$, 1.7, and 1.2 for field-aligned, intermediate, and diffuse distributions, respectively.

[54] It should be noted that the results of *Bonifazi and Moreno* [1981, Figure 4] show that the speeds of diffuse, intermediate, and field-aligned distributions exhibit significant overlap and variability about the average values. This is reflected in more recent observations. For example, although *Bonifazi and Moreno* [1981] quote an average $v_b/v_{sw} \sim 2$ for field-aligned distributions, *Meziane et al.* [2004] have observed a field-aligned distribution with $v_b/v_{sw} = 1.68$, which is less than the average intermediate distribution speed reported by Bonifazi and Moreno. In addition, the actual beam speed is also a function of shock geometry and depends on the manner in which the beam is produced. A detailed model of the beam production process would allow the predicted and inferred beam speeds to be compared more closely, but such a study is beyond the scope of this paper.

[55] The waves that arise from beams with lower inferred $v_b/v_{sw}$ may have, for example, been generated by ions that

were specularly reflected at the shock and are gyrophase mixing [cf., e.g., *Gurgiolo et al.*, 1983; *Thomsen et al.*, 1985]. In their study of the qualitative association of gyrating and intermediate ion distributions with upstream low-frequency wave activity, *Fuselier et al.* [1986b] noted that some intermediate distributions identified on the basis of energy-time spectrograms [*Bonifazi and Moreno*, 1981] may in fact have been gyrating. An extension of this work would be to examine the detailed three-dimensional ion data to determine the proportion of the wave observations occurring in conjunction with either gyrophase bunched, gyrotropic, or intermediate beam distributions. Since thus far, detailed case studies have concentrated on the nonlinear trapping of field-aligned beams [*Mazelle et al.*, 2003], we suggest that examples of waves associated with intermediate and gyrotropic distributions be analyzed in a similar manner.

[56] Several questions remain. It would be of interest to investigate how the wave properties change with wave amplitude, for example examining the wave polarization as a function of wave amplitude, the wave amplitude as a function of $\theta_{kB}$, and the wave amplitude as a function of predicted beam speed. It would also be of interest to see how the wave properties depend on the plasma beta, since this is thought to control wave properties in the kinetic picture [*Krauss-Varban et al.*, 1994]. More detailed studies of waves inferred to be in resonance with slow beams are also planned. Further work is required to establish experimentally the properties of ULF wave modes excited by gyrophase bunched distributions, such as those produced by specular reflection at the quasi-parallel shock [*Gurgiolo et al.*, 1983; *Thomsen et al.*, 1985]; multispacecraft case studies similar to *Mazelle et al.* [2003] are required to fully address this question. It would also be of interest to attempt to study the evolution of wave packets: at large separations, it may be possible to map waves observed by one Cluster spacecraft to waves observed at a later time by a second Cluster spacecraft in a different location. Changes in the wave properties may reveal aspects of the nonlinear evolution of the wave. This may provide insight into the nonlinear development of the wave generation process.

[57] **Acknowledgments.** David Sibeck provided many useful comments and his constructive criticism was appreciated. This research was conceived while JPE held a PPARC studentship at Imperial College London. JPE holds a National Research Council Research Associateship Award at NASA GSFC. JPE and CM would also like to thank the International Space Science Institute for their hospitality.

[58] Shadia Rifai Habbal thanks both referees for their assistance in evaluating this paper.

## References

Asbridge, J. R., S. J. Bame, and I. B. Strong (1968), Outward flow of protons from the Earth's bow shock, *J. Geophys. Res.*, *73*, 5777–5782.

Balogh, A., et al. (2001), The Cluster magnetic field investigation: Overview of inflight performance and initial results, *Ann. Geophys.*, *19*, 1207–1217.

Barnes, A. (1970), Theory of generation of bow-shock-associated hydromagnetic waves in the upstream interplanetary medium, *Cosmic Electrodyn.*, *1*, 90–114.

Bendat, J. S., and A. G. Piersol (1986), *Random Data Analysis and Measurement Procedures*, John Wiley, Hoboken, N. J.

Bonifazi, C., and G. Moreno (1981), Reflected and diffuse ions backstreaming from the Earth's bow shock: 1. Basic properties, *J. Geophys. Res.*, *86*, 4397–4404.

Brinca, A. L. (1991), Cometary linear instabilities: From profusion to perspective, in *Cometary Plasma Processes*, *Geophys. Monogr. Ser.*, vol. 61, edited by A. D. Johnstone, pp. 211–221, AGU, Washington, D. C.

Burgess, D. (1997), What do we really know about upstream waves?, *Adv. Space Res.*, *20*(4–5), 673–682.

Burgess, D., and S. J. Schwartz (1984), The dynamics and upstream distributions of ions reflected at the Earth's bow shock, *J. Geophys. Res.*, *89*, 7407–7422.

Devore, J. L. (2000), *Probability and Statistics for Engineering and the Sciences*, Duxbury, Pacific Grove, Calif.

Eastwood, J. P., A. Balogh, M. W. Dunlop, T. S. Horbury, and I. Dandouras (2002), Cluster observations of fast magnetosonic waves in the terrestrial foreshock, *Geophys. Res. Lett.*, *29*(22), 2046, doi:10.1029/2002GL015582.

Eastwood, J. P., A. Balogh, C. Mazelle, I. Dandouras, and H. Rème (2004), Oblique propagation of 30 s period fast magnetosonic foreshock waves: A Cluster case study, *Geophys. Res. Lett.*, *31*, L04804, doi:10.1029/2003GL018897.

Eastwood, J. P., A. Balogh, E. A. Lucek, C. Mazelle, and I. Dandouras (2005), Quasi-monochromatic ULF foreshock waves as observed by the four-spacecraft Cluster mission: 2. Oblique propagation, *J. Geophys. Res.*, *110*, A11220, doi:10.1029/2004JA010618.

Edmiston, J. P., C. F. Kennel, and D. Eichler (1982), Escape of heated ions upstream of quasi-parallel shocks, *Geophys. Res. Lett.*, *9*, 531–534.

Eriksson, A. I. (1998), Spectral analysis, in *Analysis Methods for Multi-Spacecraft Data*, edited by G. Paschmann and P. W. Daly, pp. 5–42, Int. Space Sci. Inst., Bern, Switzerland.

Escoubet, C. P., M. Fehringer, and M. L. Goldstein (2001), The Cluster mission, *Ann. Geophys.*, *19*, 1197–1200.

Fairfield, D. H. (1969), Bow shock associated waves observed in the far upstream interplanetary medium, *J. Geophys. Res.*, *74*, 3541–3553.

Fazakerley, A. N., A. J. Coates, and M. W. Dunlop (1995), Observations of upstream ions, solar wind ions and electromagnetic waves in the Earth's foreshock, *Adv. Space Res.*, *15*(8–9), 103–106.

Fitzenreiter, R. J. (1995), The electron foreshock, *Adv. Space Res.*, *15*(8–9), 9–27.

Fuselier, S. A. (1994), Suprathermal ions upstream and downstream from the Earth's bow shock, in *Solar Wind Sources of Magnetospheric Ultra-Low-Frequency Waves*, *Geophys. Monogr. Ser.*, vol. 81, edited by M. J. Engebretson, K. Takahashi, and M. Scholer, pp. 107–119, AGU, Washington D. C.

Fuselier, S. A. (1995), Ion distributions in the Earth's foreshock upstream from the bow shock, *Adv. Space Res.*, *15*(8–9), 43–52.

Fuselier, S. A., M. F. Thomsen, S. P. Gary, S. J. Bame, C. T. Russell, and G. K. Parks (1986a), The phase relationship between gyrophase-bunched ions and MHD-like waves, *Geophys. Res. Lett.*, *13*, 60–63.

Fuselier, S. A., M. F. Thomsen, J. T. Gosling, S. J. Bame, and C. T. Russell (1986b), Gyrating and intermediate ion distributions upstream from the Earth's bow shock, *J. Geophys. Res.*, *91*, 91–99.

Gary, S. P. (1993), *Theory of Space Plasma Microinstabilities*, Cambridge Univ. Press, New York.

Gosling, J. T., M. F. Thomsen, S. J. Bame, W. C. Feldman, G. Paschmann, and N. Sckopke (1982), Evidence for specularly reflected ions upstream from the quasi-parallel shock, *Geophys. Res. Lett.*, *9*, 1333–1336.

Greenstadt, E. W., G. Le, and R. J. Strangeway (1995), ULF waves in the foreshock, *Adv. Space Res.*, *15*(8–9), 71–84.

Gurgiolo, C., G. K. Parks, and B. H. Mauk (1983), Upstream gyrophase bunched ions: A mechanism for creation at the bow shock and the growth of velocity space structure through gyrophase mixing, *J. Geophys. Res.*, *88*, 9093–9100.

Hoppe, M. M., and C. T. Russell (1982), Particle acceleration at planetary bow shock waves, *Nature*, *295*, 41–42.

Hoppe, M. M., and C. T. Russell (1983), Plasma rest frame frequencies and polarizations of the low-frequency upstream waves: ISEE 1 and 2 observations, *J. Geophys. Res.*, *88*, 2021–2028.

Hoshino, M., and T. Terasawa (1985), Numerical study of the upstream wave excitation mechanism: 1. Nonlinear phase bunching of beam ions, *J. Geophys. Res.*, *90*, 57–64.

Krauss-Varban, D., N. Omidi, and K. B. Quest (1994), Mode properties of low frequency waves: Kinetic theory versus Hall-MHD, *J. Geophys. Res.*, *99*, 5987–6010.

Le, G., and C. T. Russell (1994), The morphology of ULF waves in the Earth's foreshock, in *Solar Wind Sources of Magnetospheric Ultra-Low-Frequency Waves*, *Geophys. Monogr. Ser.*, vol. 81, edited by M. J. Engebretson, K. Takahashi, and M. Scholer, pp. 87–98, AGU, Washington, D. C.

Mazelle, C., D. Le Quéau, and K. Meziane (2000), Nonlinear wave-particle interaction upstream from the Earth's bow shock, *Nonlinear Proc. Geophys.*, *7*, 185–190.

Mazelle, C., et al. (2003), Production of gyrating ions from nonlinear wave-particle interaction upstream from the Earth's bow shock: A case study from Cluster-CIS, *Planet. Space Sci.*, *51*, 785–795.

Means, J. D. (1972), Use of the three-dimensional covariance matrix in analyzing the polarization properties of plane waves, *J. Geophys. Res.*, *77*, 5551–5559.

Meziane, K., and C. d'Uston (1998), A statistical study of the upstream intermediate ion boundary in the Earth's foreshock, *Ann. Geophys.*, *16*, 125–133.

Meziane, K., C. Mazelle, R. P. Lin, D. Le Quéau, D. E. Larson, G. K. Parks, and R. P. Lepping (2001), Three-dimensional observations of gyrating ion distributions far upstream from the Earth's bow shock and their association with low-frequency waves, *J. Geophys. Res.*, *106*, 5731–5742.

Meziane, K., et al. (2004), Simultaneous observations of field-aligned beams and gyrating ions in the terrestrial foreshock, *J. Geophys. Res.*, *109*, A05107, doi:10.1029/2003JA010374.

Möbius, E., et al. (2001), Observations of the spatial and temporal structure of field-aligned beam and gyrating ring distributions at the quasi-perpendicular bow shock with Cluster CIS, *Ann. Geophys.*, *19*, 1411–1420.

Narita, Y., K.-H. Glassmeier, S. Schafer, U. Motschmann, K. Sauer, I. Dandouras, K.-H. Fornacon, E. Georgescu, and H. Rème (2003), Dispersion analysis of ULF waves in the foreshock using cluster data and the wave telescope technique, *Geophys. Res. Lett.*, *30*(13), 1710, doi:10.1029/2003GL017432.

Paschmann, G., N. Sckopke, S. J. Bame, J. R. Asbridge, J. T. Gosling, C. T. Russell, and E. W. Greenstadt (1979), Association of low frequency waves with suprathermal ions in the upstream solar wind, *Geophys. Res. Lett.*, *6*, 209–212.

Paschmann, G., N. Sckopke, J. R. Asbridge, S. J. Bame, and J. T. Gosling (1980), Energization of solar wind ions by reflection from the Earth's bow shock, *J. Geophys. Res.*, *85*, 4689–4693.

Peredo, M., J. A. Slavin, E. Mazur, and S. A. Curtis (1995), Three-dimensional position and shape of the bow shock and their variation with Alfvénic, sonic and magnetosonic Mach numbers and interplanetary magnetic field orientation, *J. Geophys. Res.*, *100*, 7907–7916.

Pinçon, J. L., and U. Motschmann (1998), Multi-spacecraft filtering: General framework, in *Analysis Methods for Multi-Spacecraft Data*, edited by G. Paschmann and P. W. Daly, pp. 65–78, Int. Space Sci. Inst., Bern, Switzerland.

Rème, H., et al. (2001), First multispacecraft ion measurements in and near the Earth's magnetosphere with the identical Cluster ion spectrometry (CIS) experiment, *Ann. Geophys.*, *19*, 1303–1354.

Schwartz, S. J. (1998), Shock and discontinuity normals, Mach numbers and related parameters, in *Analysis Methods for Multi-Spacecraft Data*, edited by G. Paschmann and P. W. Daly, pp. 249–270, Int. Space Sci. Inst., Bern, Switzerland.

Schwartz, S. J., and D. Burgess (1984), On the theoretical/observational comparison of field-aligned ion beams in the Earth's foreshock, *J. Geophys. Res.*, *89*, 2381–2384.

Song, P., and C. T. Russell (1999), Time series data analyses in space plasmas, *Space Sci. Rev.*, *87*, 387–463.

Sonnerup, B. U. Ö (1969), Acceleration of particles reflected at a shock front, *J. Geophys. Res.*, *74*, 1301–1304.

Sonnerup, B. U. Ö., and M. Scheible (1998), Minimum and maximum variance analysis, in *Analysis Methods for Multi-Spacecraft Data*, edited by G. Paschmann and P. W. Daly, pp. 185–220, Int. Space Sci. Inst., Bern, Switzerland.

Thomsen, M. F. (1985), Upstream suprathermal ions, in *Collisionless Shocks in the Heliosphere: Reviews of Current Research*, *Geophys. Monogr. Ser.*, vol. 35, edited by B. T. Tsurutani and R. G. Stone, pp. 253–270, AGU, Washington, D. C.

Thomsen, M. F., J. T. Gosling, S. J. Bame, and C. T. Russell (1985), Gyrating ions and large-amplitude monochromatic MHD waves upstream of the Earth's bow shock, *J. Geophys. Res.*, *90*, 267–273.

Watanabe, Y., and T. Terasawa (1984), On the excitation mechanism of the low-frequency upstream waves, *J. Geophys. Res.*, *89*, 6623–6630.

A. Balogh and E. A. Lucek, Space and Atmospheric Physics, Blackett Laboratory, Imperial College London, Prince Consort Road, London SW7 2BW, UK.

I. Dandouras and C. Mazelle, Centre d'Etude Spatiale des Rayonnements, Centre National de la Recherche Scientifique, 9 avenue du colonel Roche, F-31028 Toulouse, France.

J. P. Eastwood, Laboratory for Solar and Space Physics, Geospace Physics Branch, NASA Goddard Space Flight Center, Code 612.3, Greenbelt, MD 20771, USA. (jonathan.p.eastwood.1@gsfc.nasa.gov)